ZFP423 controls EBF2 coactivator recruitment and PPARγ occupancy to determine the thermogenic plasticity of adipocytes

Mengle Shao,[1,5,6] Qianbin Zhang,[1,6] Ashley Truong,[1] Bo Shan,[1] Lavanya Vishvanath,[1] Lin Li,[2,3] Patrick Seale,[4] and Rana K. Gupta[1]

[1]Touchstone Diabetes Center, Department of Internal Medicine, University of Texas Southwestern Medical Center, Dallas, Texas 75390, USA; [2]Department of Pediatrics, [3]Department of Internal Medicine, Children's Research Institute, Center for Regenerative Science and Medicine, University of Texas Southwestern Medical Center, Dallas, Texas 75390, USA; [4]Institute for Diabetes, Obesity, and Metabolism, Department of Cell and Developmental Biology, Perelman School of Medicine at the University of Pennsylvania, Philadelphia, Pennsylvania 19104, USA

Energy-storing white adipocytes maintain their identity by suppressing the energy-burning thermogenic gene program of brown and beige adipocytes. Here, we reveal that the protein–protein interaction between the transcriptional coregulator ZFP423 and brown fat determination factor EBF2 is essential for restraining the thermogenic phenotype of white adipose tissue (WAT). Disruption of the ZFP423–EBF2 protein interaction through CRISPR–Cas9 gene editing triggers widespread "browning" of WAT in adult mice. Mechanistically, ZFP423 recruits the NuRD corepressor complex to EBF2-bound thermogenic gene enhancers. Loss of adipocyte *Zfp423* induces an EBF2 NuRD-to-BAF coregulator switch and a shift in PPARγ occupancy to thermogenic genes. This shift in PPARγ occupancy increases the antidiabetic efficacy of the PPARγ agonist rosiglitazone in obesity while diminishing the unwanted weight-gaining effect of the drug. These data indicate that ZFP423 controls EBF2 coactivator recruitment and PPARγ occupancy to determine the thermogenic plasticity of adipocytes and highlight the potential of therapeutically targeting transcriptional brakes to induce beige adipocyte biogenesis in obesity.

[*Keywords*: EBF2; PPARγ; ZFP423; beige adipocytes; rosiglitazone; white adipocytes]

Supplemental material is available for this article.

Received June 26, 2021; revised version accepted September 7, 2021.

Eutherian mammals harbor distinct types of adipocytes that differentially impact energy balance and nutrient homeostasis (Rosen and Spiegelman 2014). White adipocytes contain large, unilocular fat droplets and represent the principal site for long-term energy storage in the form of triglyceride. Brown adipocytes function to catabolize stored lipids and produce heat, thus contributing to energy expenditure. Brown adipocytes are distinguished by their multilocular lipid droplet appearance, high mitochondrial content, and expression of *uncoupling protein 1* (*Ucp1*).

Remarkably, certain WAT depots possess the capacity to adopt a catabolic thermogenic phenotype reminiscent of brown adipose tissue (BAT) (Lončar 1991). This "browning" of WAT is characterized by the emergence of fundamentally distinct UCP1+ beige adipocytes (Wu et al. 2012). Upon exposure to cold temperatures or other settings involving activation of the β-adrenergic signaling cascade, dormant unilocular beige adipocytes become active and new beige adipocytes emerge from resident adipocyte progenitors (Barbatelli et al. 2010; Rosenwald et al. 2013; Wang et al. 2013; Lee et al. 2015; Vishvanath et al. 2016; Roh et al. 2018; Shao et al. 2019). Rodent studies indicate that thermogenic remodeling of WAT can regulate glucose and lipid homeostasis and increase energy expenditure (Seale et al. 2011; Harms and Seale 2013; Kajimura et al. 2015; Shao et al. 2016). In humans, the presence of active thermogenic adipose tissue is similarly associated with cardiometabolic benefits (Becher et al. 2021). As such, driving the production and activity of thermogenic

[5]Present address: The Center for Microbes, Development, and Health, Institut Pasteur of Shanghai, Chinese Academy of Sciences, Shanghai 200031, China.
[6]These authors contributed equally to this work.
Corresponding author: rana.gupta@utsouthwestern.edu
Article published online ahead of print. Article and publication date are online at http://www.genesdev.org/cgi/doi/10.1101/gad.348780.121.

adipocytes may be a promising strategy to improve cardiometabolic health in obesity.

The transcriptional networks controlling the establishment and maintenance of the distinct adipocyte lineages in vivo are still being defined. PPARγ, along with other differentiation-linked transcription factors, represents a core transcriptional network critical for the development and maintenance of adipocytes (Mota de Sa et al. 2017); however, additional factors operate alongside PPARγ to specify an energy-storing versus energy-burning adipocyte fate (Shao and Gupta 2019; Shapira and Seale 2019). In particular, the transcription factor early B-cell factor 2 (EBF2) activates many key thermogenic genes in adipocytes (Rajakumari et al. 2013; Wang et al. 2014; Stine et al. 2016). EBF2 recruits a tissue-selective BAF chromatin remodeling complex to thermogenic gene enhancers, thereby regulating chromatin accessibility and PPARγ occupancy (Shapira et al. 2017).

White adipocytes harbor mechanisms to actively suppress the thermogenic gene program (Villanueva et al. 2013; Pearson et al. 2019; Shao and Gupta 2019). Our group has previously identified the multi-C2H2 zinc finger transcriptional coregulator ZFP423 as a potent suppressor of the thermogenic phenotype in white adipocytes (Shao et al. 2016; Hepler et al. 2017). Inducible deletion of *Zfp423* in adipocytes of adult mice housed at room temperature leads to a widespread accumulation of UCP1+ multilocular beige adipocytes within the inguinal WAT (iWAT) depot. Lineage tracing reveals that beige adipocytes in this model arise from mature *Adiponectin*-expressing *Zfp423*-deficient adipocytes. This thermogenic remodeling confers resistance to diet-induced obesity and insulin resistance. Moreover, deletion of adipocyte *Zfp423* in mice with established obesity unlocks the thermogenic capacity of white adipocytes and allows pharmacological β-adrenergic receptor activation to drive weight loss (Shao et al. 2016). ZFP423 interacts with EBF2 to inhibit its ability to activate the thermogenic gene program in adipocytes (Shao et al. 2016); however, the physiological importance of this protein–protein interaction in controlling the thermogenic capacity of white adipocytes, along with the molecular mechanism by which ZFP423 regulates EBF2 transcriptional activity, has remained unclear.

Here, we demonstrate that genetic disruption of the ZFP423–EBF protein interaction through CRISPR/Cas9 gene editing is sufficient to trigger widespread thermogenic remodeling of WAT in adult mice. Biochemical and molecular approaches, including mass spectrometry, genome-wide chromatin immunoprecipitation assays (ChIP-seq), and chromatin affinity purification (ChAP-seq) of endogenous genetically tagged ZFP423, reveal that ZFP423 recruits the NuRD corepressor components to EBF2 target enhancers to suppress thermogenic gene expression in white adipocytes. Remarkably, inducible deletion of *Zfp423* in mature adipocytes induces a NuRD-to-BAF complex coregulator switch onto EBF2 along with a notable shift in PPARγ occupancy to thermogenic gene enhancers. This shift in PPARγ occupancy to thermogenic genes increases the antidiabetic capacity of rosiglitazone in obesity while diminishing the weight-gaining side effects of the drug. Altogether, these data reveal that the ZFP423–EBF protein interaction is critical for suppression of the thermogenic gene program in white adipocytes via limiting EBF2 coactivator engagement and its ability to promote PPARγ occupancy at thermogenic genes. These data highlight the potential for targeting thermogenic transcriptional brakes in adipocytes as part of a therapeutic strategy to induce thermogenic WAT remodeling and improve metabolic health in obesity.

Results

ZFs 29–30 of ZFP423 mediate its EBF2 interaction and antithermogenic function

ZFP423 physically interacts with EBF2 and inhibits its ability to transactivate thermogenic genes in adipocytes (Shao et al. 2016). The last four C-terminal C2H2 zinc fingers (ZFs) of ZFP423 (ZFs 26–30) mediate its direct interaction with the EBF family of transcription factors (Fig. 1A; Hata et al. 2000; Shao et al. 2016). We mapped the ZF(s) within the C-terminal region of ZFP423 that are essential for the ZFP423–EBF2 interaction. We engineered mutant forms of *Zfp423* designed to disrupt individual C2H2 ZF motifs through histidine-to-asparagine substitutions (Fig. 1A). We used retroviral vectors to express either full-length ZFP423 (ZFs 1–30), a previously described variant lacking the C-terminal zinc fingers (ZFs 1–25) (Gupta et al. 2010), or variants with disruptions in either ZF 28 (H1224N), ZF 29 (H1255N), or ZF 30 (H1285N) in immortalized brown stromal vascular cells. Coimmunoprecipitation assays revealed that disruption of ZF 28 did not impact the ability of EBF2 to interact with ZFP423, whereas disruption of ZF 29 or 30 attenuated this interaction without affecting ZFP423 protein expression (Fig. 1B). Notably, variants of ZFP423 that did not interact with EBF2 failed to suppress thermogenic gene expression in adipocytes (Fig. 1C). In particular, the mutation of ZF 30 completely abrogated the ability of ZFP423 to suppress thermogenic genes while having no effect on adipocyte differentiation per se (Fig. 1C). Disruption of ZF 29 (H1255N) partially blocked the ability of ZFP423 to interact with EBF2 and partially attenuated the capacity for ZFP423 to suppress thermogenic gene expression (Fig. 1C). Importantly, disrupting ZF 30 did not impact other functions of ZFP423. ZFP423 promotes preadipocyte lineage commitment by interacting with SMADs through a well-characterized SMAD-binding domain (SBD) and amplifying bone morphogenic protein (BMP) signaling (Supplemental Fig. S1A; Hata et al. 2000; Gupta et al. 2010). ZFP423 H1285N maintained its ability to drive *Pparg* expression in NIH 3T3 cells and amplified the effects of BMP4 in activating *Pparg* expression (Supplemental Fig. S1B).

Genetic disruption of the adipocyte ZFP423–EBF2 interaction leads to thermogenic WAT remodeling

To determine the physiological importance of the adipocyte ZFP423–EBF2 interaction we used CRISPR–Cas9 gene editing to derive a mouse model in which the

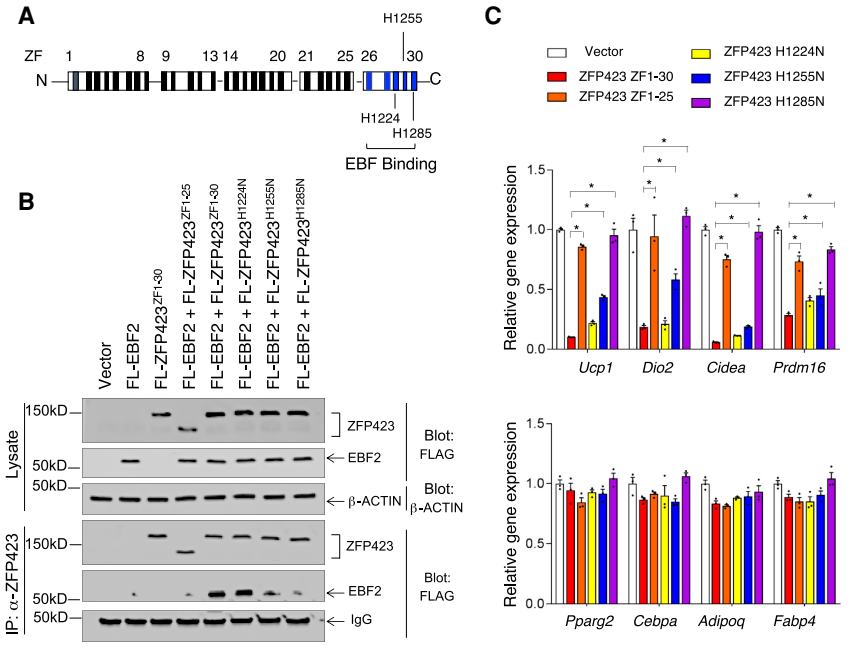

Figure 1. Identification of zinc fingers (ZFs) mediating ZFP423 interaction with EBF2. (*A*) Schematic representation of 30 zinc finger (ZF) motifs within murine ZFP423. The previously identified EBF family interaction domain is highlighted in blue. ZFs 28–30 were individually mutated through histidine-to-asparagine substitutions at the indicated histidine residues. (*B*) Western blot analysis of the indicated proteins in whole-cell lysates (*top*) and ZFP423 immunoprecipitates (*bottom*) from differentiated immortalized brown stromal vascular cells following sequential transduction with retrovirus carrying *Ebf2* and then retrovirus expressing FLAG-tagged (FL) ZFP423 variants. (*C*) Relative mRNA levels of thermogenic genes (*top*) and common adipocyte-selective genes (*bottom*) in cultures of in vitro differentiated immortalized brown stromal vascular cells expressing the indicated ZFP423 variants. Bars represent mean + SEM. (*) $P < 0.05$ by one-way ANOVA. $n = 3$ biological replicates.

H1285N mutation is encoded into the endogenous *Zfp423* locus. We simultaneously engineered the mutant allele to encode a 15-amino-acid sequence (GLNDIFEAQ**K**IEWHE) at the C terminus that can be specifically biotinylated by the *E. coli* enzyme BirA (termed "Avi tag") (Supplemental Fig. S2A; Beckett et al. 1999). In a parallel strain, we also engineered the wild-type *Zfp423* allele to encode Avi-tagged ZFP423 (Supplemental Fig. S2A). Global homozygous *Zfp423* knockout mice die shortly after birth and exhibit severe defects in the development of midline structures of the brain (Alcaraz et al. 2006; Warming et al. 2006). Mice heterozygous (*Zfp423*$^{\text{WT-Avi/+}}$) or homozygous (*Zfp423*$^{\text{WT-Avi/ WT-Avi}}$) for the *Zfp423*$^{\text{WT-Avi}}$ allele mice were viable and fertile and did not display any gross physiological abnormalities in comparison with wild-type littermates (*Zfp423*$^{+/+}$). Thus, insertion of the Avi tag did not create a dominant-negative or null allele. Likewise, mice heterozygous (*Zfp423*$^{\text{H1285N-Avi/+}}$) for the *Zfp423*$^{\text{H1285N-Avi}}$ allele were indistinguishable from wild-type littermates. These data imply that ZFP423 H1285N is not acting as a dominant negative. In contrast, animals homozygous for the H1285N mutation (*Zfp423*$^{\text{H1285N-Avi/ H1285N-Avi}}$) did not survive beyond postnatal day 1 or 2. This is in line with prior studies indicating the importance of the ZFP423–EBF interaction in the embryonic development of the CNS (Roby et al. 2012).

To confirm the expression of ZFP423$^{\text{WT-Avi}}$ and ZFP423$^{\text{H1285N-Avi}}$ in adipocytes we crossed *Zfp423*$^{\text{WT-Avi/+}}$ mice or *Zfp423*$^{\text{H1285N-Avi/+}}$ mice to a model in which BirA is expressed in mature adipocytes in a CRE- and doxycycline (Dox)-dependent manner (Supplemental Fig. S2B). This new model consists of one transgene that expresses the reverse tetracycline transactivator (rtTA) under the control of a 5.4-kb promoter fragment of the *adiponectin* locus (Wang et al. 2010), another transgene in which CRE recombinase is expressed from a promoter containing the Tet response element (TRE-Cre), and modified *Rosa26R* alleles expressing *E. coli* BirA in a CRE-dependent manner (*Rosa26R*$^{\textit{lox-STOP-lox-BirA}}$) (Johnson et al. 2017). Feeding of Dox-containing chow diet (Dox-chow) to adult quadruple-transgenic (*Adiponectin*$^{\textit{rtTA}}$; *TRE-Cre*; *Rosa26R*$^{\textit{lox-STOP-lox-BirA}}$; *Zfp423*$^{\text{WT-Avi/+}}$ or *Adiponectin*$^{\textit{rtTA}}$; *TRE-Cre*; *Rosa26R*$^{\textit{lox-STOP-lox-BirA}}$; *Zfp423*$^{\text{H1285N-Avi/+}}$) mice triggers CRE-mediated activation of BirA expression specifically in terminally differentiated adipocytes and subsequent biotinylation of Avi-tagged ZFP423. Upon 7 d of Dox-chow feeding, we readily detected both genetically modified ZFP423 proteins in iWAT lysates using fluorescence-conjugated streptavidin (Supplemental Fig. S2C). Importantly, both ZFP423$^{\text{WT-Avi}}$ and ZFP423$^{\text{H1285N-Avi}}$ proteins were detectable at comparable levels (Supplemental Fig. S2C).

We asked whether ZFP423 H1285N can suppress the thermogenic phenotype of adipose tissue in vivo. We derived mice in which the addition of Dox-chow results in the inactivation of one *Zfp423* allele in adipocytes, with the remaining allele expressing either ZFP423$^{\text{WT-Avi}}$ (termed "Adipo-*Zfp423*$^{\text{WT-Avi}}$" mice) or ZFP423$^{\text{H1285N-Avi}}$ (termed "Adipo-*Zfp423*$^{\text{H1285N-Avi}}$" mice) (Fig. 2A). We placed 8-wk-old male animals on Dox-chow for 4 wk while housed at room temperature (22°C). Consistent with our prior studies, we observed widespread morphological and molecular browning of iWAT depots and increased thermogenic gene expression in epididymal WAT (eWAT) from animals lacking adipocyte *Zfp423* (*Zfp423*-iAKO mice) (Fig. 2B–D; Supplemental Fig. S3). These phenotypes were not observed in animals heterozygous for either the *Zfp423*-null allele (*Adiponectin*$^{\textit{rtTA}}$; *TRE-Cre*; *Zfp423*$^{+/\textit{loxP}}$ animals) or carrying the *Zfp423*$^{\text{WT-Avi}}$ allele, indicating that one active wild-type allele of *Zfp423* is sufficient to maintain the white adipocyte phenotype and suppress UCP1 expression.

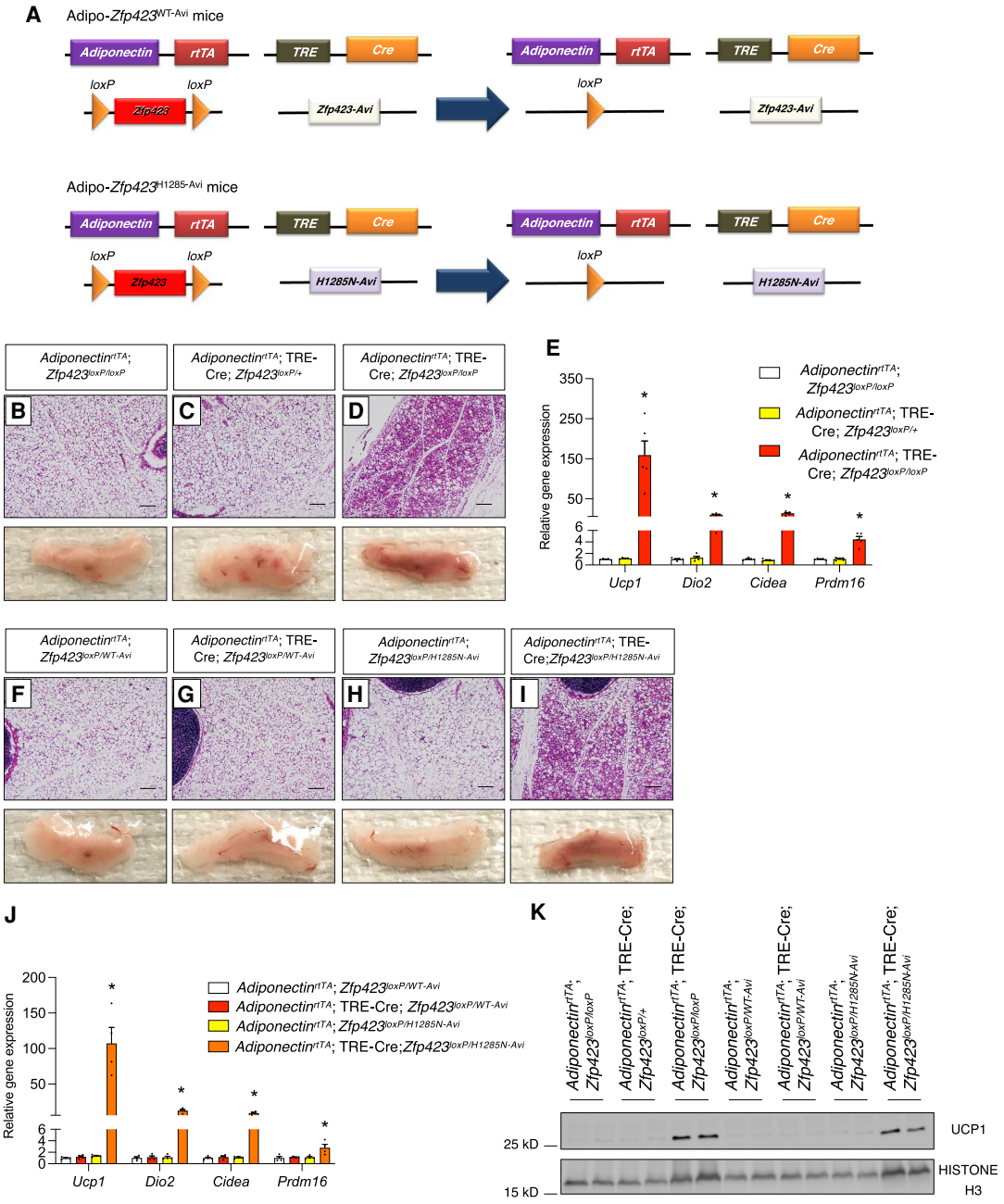

Figure 2. Genetic disruption of the ZFP423–EBF2 interaction in adipocytes leads to thermogenic WAT remodeling. (*A*) Components of the Adipo-*Zfp423*$^{\text{WT-Avi}}$ and Adipo-*Zfp423*$^{\text{H1285N-Avi}}$ mouse models. Quadruple transgenic mice consist of *Adiponectin*$^{\text{rtTA}}$ and *TRE-Cre* transgenes, one floxed Zfp423 allele (*Zfp423*$^{lopx/+}$), and one allele engineered to express either ZFP423$^{\text{WT-Avi}}$ (*Zfp423*$^{\text{WT-Avi/+}}$) or ZFP423$^{\text{H1285N-Avi}}$ (*Zfp423*$^{\text{H1285N-Avi/+}}$). Dox-chow diet feeding results in the inactivation of one *Zfp423* allele in *adiponectin*-expressing mature adipocytes, with the other allele expressing either ZFP423$^{\text{WT-Avi}}$ in Adipo-*Zfp423*$^{\text{WT-Avi}}$ mice or ZFP423$^{\text{H1285N-Avi}}$ in Adipo-*Zfp423*$^{\text{H1285N-Avi}}$ mice. (*B–D*) Representative bright-field images of H&E-stained sections of iWAT depots obtained from adult mice with the indicated genotypes after 4 wk of Dox-chow diet feeding at room temperature. Scale bar, 200 µm. Representative photographs of dissected whole iWAT depots are shown. (*E*) Relative mRNA levels of thermogenic genes in iWAT from adult mice with the indicated genotypes after 4 wk of Dox-chow diet feeding at room temperature. Bars represent mean ± SEM. (*) $P < 0.05$ for *Adiponectin*$^{\text{rtTA}}$; *Zfp423*$^{loxp/loxP}$ versus *Adiponectin*$^{\text{rtTA}}$; TRE-Cre; *Zfp423*$^{loxP/loxP}$ by one-way ANOVA. $n = 5$ biological replicates. (*F–I*) Representative bright-field images of H&E-stained sections of iWAT depots obtained from adult mice with the indicated genotypes after 4 wk of DOX-chow diet feeding at room temperature. Scale bar, 200 µm. Representative photographs of dissected whole iWAT depots are shown. (*J*) Relative mRNA levels of thermogenic genes in iWAT from adult mice with the indicated genotypes after 4 wk of Dox-chow diet feeding at room temperature. Bars represent mean ± SEM. (*) $P < 0.05$ for *Adiponectin*$^{\text{rtTA}}$; *Zfp423*$^{loxp/WT\text{-}Avi}$ versus *Adiponectin*$^{\text{rtTA}}$; TRE-Cre; *Zfp423*$^{loxP/H1285N\text{-}Avi}$ by one-way ANOVA. $n = 4$ biological replicates. (*K*) Western blot analysis of UPC1 protein levels in whole iWAT depots isolated from adult mice with the indicated genotypes after 4 wk of Dox-chow diet feeding at room temperature.

Importantly, iWAT depots from mice carrying one functionally wild-type *Zfp423* allele and one *Zfp423*$^{H1285N\text{-}Avi}$ allele are morphologically indistinguishable from control animals (Fig. 2F–H). This further indicates that Zfp423$^{H1285N\text{-}Avi}$ is not acting as a dominant negative. Remarkably, iWAT depots of Adipo-*Zfp423*$^{H1285N\text{-}Avi}$ mice, which only express *Zfp423*$^{H1285N\text{-}Avi}$ in adipocytes, resemble the iWAT depots of the adipocyte *Zfp423* knockout animals. iWAT depots of Adipo-*Zfp423*$^{H1285N\text{-}Avi}$ mice contain large regions of multilocular adipocytes and express key thermogenic genes and UCP1 protein (Fig. 2I–K). These data indicate that ZFP423$^{H1285N\text{-}Avi}$ cannot maintain the inguinal white adipocyte phenotype. Moreover, we also observed an increase in thermogenic gene expression in eWAT depots of Adipo-*Zfp423*$^{H1285N\text{-}Avi}$ mice maintained at room temperature (Supplemental Fig. S3). Collectively, these data further implicate the ZFP423–EBF interaction as a key protein–protein interaction responsible for suppressing the thermogenic phenotype of white adipose tissue in mice.

Endogenous ZFP423 co-occupies EBF2 target genes in adipocytes

The precise mechanisms by which ZFP423 inhibits EBF2 activity are unclear. To begin to address this, we asked whether ZFP423 localizes to EBF2 target genes in adipocytes. We performed chromatin affinity purification (ChAP) of the endogenous Avi-tagged ZFP423$^{WT\text{-}Avi}$ and ZFP423$^{H1285N\text{-}Avi}$ protein using streptavidin beads. We used iWAT stromal vascular cells from mice heterozygous for either the *Zfp423*$^{WT\text{-}Avi}$ allele or *Zfp423*$^{H1285N\text{-}Avi}$ allele and capable of inducible BirA expression in an adipocyte-specific manner. Following adipocyte differentiation, we induced BirA expression in adipocytes with Dox and then isolated chromatin for ChAP sequencing analysis (Fig. 3A). ChAP-seq identified 46,146 peaks occupied by ZFP423$^{WT\text{-}Avi}$ in mature adipocytes (Fig. 3B; Supplemental Data Set S1). Importantly, very few of these peaks were identified in cells lacking BirA, suggesting specificity toward targets occupied by Avi-tagged ZFP423 (Fig. 3B). Motif analysis identified the well-characterized EBF response element as the most enriched motif among genomic elements occupied by ZFP423$^{WT\text{-}Avi}$ (Fig. 3C; Supplemental Table S1). An annotated ZNF423 (human ortholog of ZFP423) binding motif bearing close resemblance to the EBF binding motif was also identified (Fig. 3C; Supplemental Table S1). Gene ontology analysis indicated that the genes occupied by ZFP423$^{WT\text{-}Avi}$ are linked to several biological processes related to fatty acid metabolism, glucose metabolism, and brown adipocyte differentiation (Supplemental Table S2). In parallel, we performed EBF2 ChIP-seq analysis to identify EBF2 targets in adipocytes (Supplemental Fig. S4A,B). ZFP423$^{WT\text{-}Avi}$ indeed co-occupied EBF2 targets in these cells (Fig. 3D). We did not observe a significant degree of enrichment of ZFP423$^{H1285\text{-}Avi}$ at EBF2 target genes, suggesting that the ability of ZFP423 to occupy EBF2 targets appears dependent on its ability to interact with EBF2 (Fig. 3D). It is important to note that ZFP423$^{H1285\text{-}Avi}$ retained its ability to occupy DNA, including non-EBF2 targets (Fig. 3B; Supplemental Data Set S2). In fact, motif analysis revealed an enrichment of specific binding motifs among targets occupied by ZFP423$^{H1285\text{-}Avi}$, including potential STAT response elements (Supplemental Table S3). Gene ontology analysis of ZFP423$^{H1285\text{-}Avi}$-occupied genes indicated an enrichment in pathways/genes related to extracellular matrix organization (Supplemental Table S4). Altogether, these

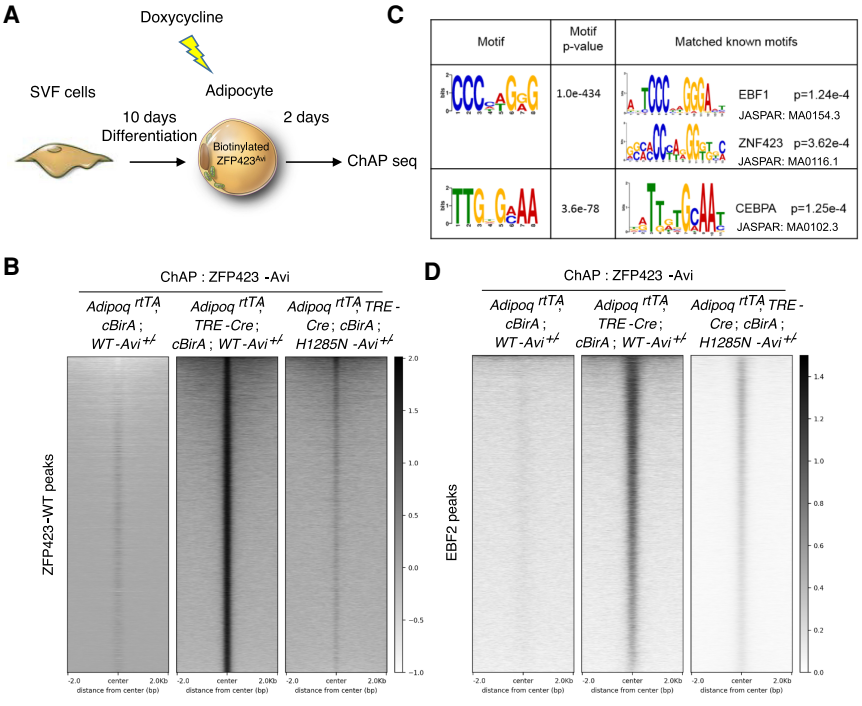

Figure 3. ZFP423 occupies EBF2 DNA binding sites in mature adipocytes. (*A*) The stromal vascular fraction (SVF) of iWAT from adult mice with the indicated genotypes was induced to differentiate in vitro. Differentiated adipocytes were treated with 5 µM Dox for 12 h to activate BirA expression and subsequent biotinylation of genetically Avi-tagged ZFP423 proteins. Forty-eight hours after Dox treatment, cells were harvested for the chromatin affinity purification (ChAP) sequencing analysis. (*B*) Heat map illustrating ZFP423$^{WT\text{-}Avi}$- and ZFP423$^{H1285N\text{-}Avi}$-occupied regions in differentiated adipocytes. (*C*) Characterized DNA-binding motifs enriched in ZFP423$^{WT\text{-}Avi}$-precipitated DNA versus ZFP423$^{H1285N\text{-}Avi}$-precipitated DNA. (*D*) Heat map illustrating ZFP423$^{WT\text{-}Avi}$ and ZFP423$^{H1285N\text{-}Avi}$ occupancy at EBF2 target sites in differentiated adipocytes.

data indicate that endogenous ZFP423 co-occupies EBF2 target genes in adipocytes, and that this association is dependent on the ZFP423–EBF2 protein interaction.

Loss of ZFP423 drives an EBF2 coregulator switch at target thermogenic genes

We next investigated whether the loss of *Zfp423* can impact EBF2 occupancy at its target genes. We used iWAT stromal vascular cells from control and *Zfp423*-iAKO mice, which allowed for Dox-inducible inactivation of *Zfp423* upon their differentiation into adipocytes. As previously reported, inducible deletion of *Zfp423* in differentiated adipocyte cultures leads to cell-autonomous activation of the thermogenic gene program within 48 h of doxycycline treatment. ChIP-seq analysis for EBF2 revealed that overall occupancy of EBF2 at its target genes was not altered in the absence of *Zfp423* (Supplemental Fig. S4A,B). This suggests that ZFP423 does not influence EBF2 chromatin binding activity, but rather its ability to activate target gene expression.

Upon DNA binding, EBF2 recruits the BRG1-containing BAF chromatin remodeling complex to brown fat-selective genes, leading ultimately to chromatin remodeling (Shapira et al. 2017). We observed that ZFP423 overexpression in brown adipocytes leads to a dissociation of the EBF2–BRG1 interaction, indicating that ZFP423 blocks EBF2 coactivator recruitment (Supplemental Fig. S4C). Transcriptional corepressors, such as ZFP423, often recruit corepressor complexes containing chromatin-modifying enzymes. Thus, we sought to identify adipocyte ZFP423-interacting partners in an unbiased manner by using affinity purification of ZFP423 complexes and mass spectrometry analysis. LC-MS/MS analysis revealed the presence of all core components of the NuRD (nucleosome remodeling deacetylase) corepressor complex in association with ZFP423 (Supplemental Data Set S3). This complex includes several chromatin remodeling factors (CHD4, MTA1/2, RBAP46/48, and MBD3), along with histone deacetylases 1 and 2 (HDAC1 and HDAC2) (Torchy et al. 2015). The presence of this complex is notable given that ZFP423 harbors a consensus "NuRD interaction domain" (NID) (Fig. 4A), which consists of 12 amino acids that directly interact with the RBAP48 subunit of the NuRD complex (Lauberth and Rauchman 2006). Our recent work on the role of ZFP423 in adipose tissue stromal cells revealed the importance of the ZFP423–NuRD complex in the regulation of stromal cell NFκB activity and inflammatory responses (Shan et al. 2020). These data suggest that the ZFP423–NuRD interaction may suppress the expression of thermogenic genes in adipocytes. All core components of the NuRD complex were readily detected by Western blot analysis of differentiated brown adipocytes (Fig. 4B). Endogenous NuRD components associate with virally expressed FLAG-ZFP423 in brown adipocyte cultures, but not with a FLAG-tagged variant of ZFP423 that is expressed but lacks the 12-amino-acid NID (FLAG-ZFP423$^{\Delta NID}$) (Fig. 4B). Notably, the NID of ZFP423 is essential for its full capacity to suppress thermogenic genes. Expression of FLAG-ZFP423$^{\Delta NID}$ in brown adipocytes cannot suppress *Ucp1*, *Cidea*, and *Dio2* as effectively as FLAG-ZFP423 (Fig. 4C). Together, these data support a role for the NuRD complex in the mechanism by which ZFP423 suppresses thermogenic gene expression.

The data above raise the possibility of an EBF2 coregulator switch occurring at target loci upon inactivation of *Zfp423*. We performed ChIP-seq analyses for BRG1 as well as the obligate NuRD component CHD4 from control and *Zfp423*-deficient adipocyte cultures 48 h after the addition of Dox (Fig. 5A). At this time point following Dox exposure, levels of thermogenic genes are sharply elevated in *Zfp423*-deficient adipocyte cultures (Fig. 5B). Consistent with the biochemical data described above, CHD4 occupies EBF2 targets in control cells expressing *Zfp423* (Fig. 5C,E). Upon inactivation of *Zfp423*, CHD4 occupancy at EBF2 sites is diminished (Fig. 5C,E). Notably, this occurs alongside an increase in the occupancy of BRG1 at EBF2 targets when *Zfp423* is removed (Fig. 5D,E). These alterations in coregulator recruitment also coincide with increases in activating histone H3K27 acetylation (Fig. 5E). It is important to note that these changes are observed within only 48 h of inducing *Zfp423* deletion in fully differentiated adipocyte cultures. Together, these data provide evidence that the loss of *Zfp423* in adipocytes activates thermogenic gene expression by inducing an EBF2 coregulator switch at target genes.

Zfp423 *deficiency triggers a shift in genome-wide PPARγ occupancy in adipocytes*

EBF2-dependent recruitment of the BAF chromatin remodeling complex to thermogenic gene enhancers increases chromatin accessibility and PPARγ occupancy (Shapira et al. 2017). Thus, we asked whether *Zfp423* deficiency triggers a shift in PPARγ occupancy. We performed PPARγ ChIP-seq assays in parallel to the aforementioned EBF2, CHD4, and BRG1 ChIP-seq experiments. In contrast to EBF2, PPARγ undergoes a remarkable shift in genomic occupancy upon induction of *Zfp423* deletion. Overall, there is a strong reduction in global PPARγ occupancy and binding at verified PPARγ target sites (Supplemental Fig. S5A, B; Supplemental Data Set S4). However, we also identified >2000 sites with increased PPARγ binding upon Zfp423 deletion, including sites bound by EBF2 at the *Ucp1* and *Ppara* loci, indicative of a shift of PPARγ binding toward key thermogenic genes (Fig. 6B; Supplemental Data Set S5). Binding at target genes common to white and brown adipocytes (e.g., *Fabp4*, *Lpl*, *Plin1*, and *Plin2*) was not substantially altered by *Zfp423* inactivation (Supplemental Fig. S5C–F). ChIP qPCR assays confirmed our ChIP-seq results. EBF2 binding at the *Ucp1* and *Ppara* genes was not impacted by *Zfp423* deletion, whereas PPARγ occupancy at these sites was enhanced (Fig. 6C). This was associated with enhanced BRG1 occupancy and diminished CHD4 binding (Fig. 6C). Collectively, these data suggest that ZFP423 regulates the thermogenic plasticity of white adipocytes by controlling EBF2-dependent coactivator assembly and PPARγ occupancy at key thermogenic genes (Fig. 6D).

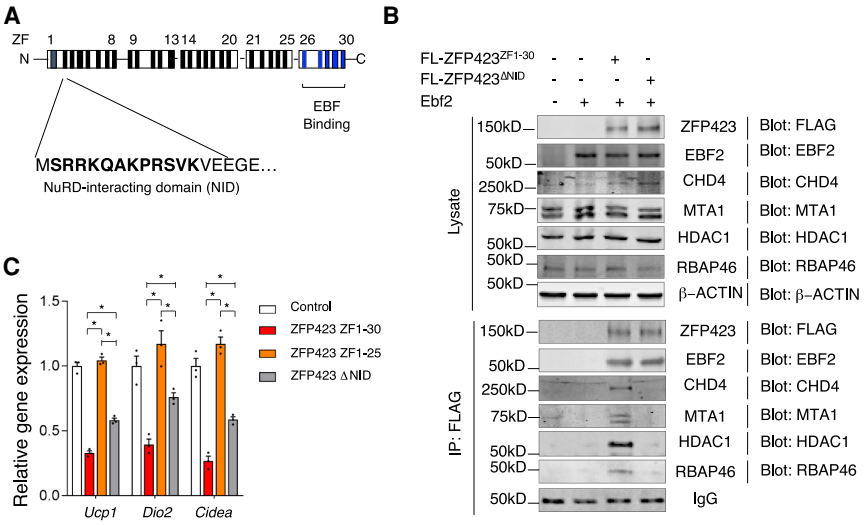

Figure 4. ZFP423 recruitment of the NuRD complex is required for its suppression of thermogenic gene expression in mature adipocytes. (*A*) Schematic representation of 30 zinc finger (ZF) motifs within murine ZFP423 with highlighted location of the N-terminal NuRD-interacting domain (NID) and C-terminal EBF binding domain. (*B*) Western blot of the indicated protein expression in whole-cell lysates (*top*) and ZFP423 immunoprecipitates (*bottom*) from differentiated transduced immortalized brown stromal vascular cells expressing EBF2 and either FLAG-tagged (FL) ZFP423$^{ZF1\text{-}30}$ or ZFP423$^{\Delta NID}$. (*C*) Relative mRNA levels of the indicated thermogenic genes in differentiated immortalized brown stromal vascular cells expressing EBF2 and either FLAG-tagged (FL) ZFP423$^{ZF1\text{-}30}$ or ZFP423$^{\Delta NID}$. Bars represent mean + SEM. (*) $P < 0.05$ by one-way ANOVA. $n = 3$ biological replicates.

Adipocyte Zfp423 *inactivation increases the antidiabetic capacity of rosiglitazone*

The shift in PPARγ occupancy toward thermogenic genes in the absence of *Zfp423* raises the question of whether the ability of PPARγ agonists to promote thermogenic remodeling could be amplified in *Zfp423*-iAKO mice. First, we confirmed by ChIP-PCR analysis that the PPARγ occupancy at key thermogenic genes (*Ucp1*, *Ppara*, and *Prdm16*) is increased in whole iWAT depots of *Zfp423*-iAKO mice maintained at room temperature on Dox-chow diet for 4 wk (Fig. 7A). Next, we placed 8-wk-old control and *Zfp423*-iAKO mice on a high-fat diet (HFD) for 10 wk. After this initial period of HFD feeding, we switched animals to a Dox-containing HFD (Dox-HFD) for 5 wk while treating animals with vehicle or the PPARγ agonist, rosiglitazone. Thus, *Zfp423* is inactivated in mature adipocytes of obese mice at the onset of drug treatment (Fig. 7B). During the 5-wk treatment period, rosiglitazone-treated *Zfp423*-iAKO mice gained much less weight than rosiglitazone-treated control animals (Fig. 7C). By the end of the 5-wk treatment period, rosiglitazone improved glucose tolerance, fasting glucose levels, and serum triglyceride levels to a much greater degree in obese *Zfp423*-iAKO mice than in control animals (Fig. 7D–E). Thus, adipocyte *Zfp423* deficiency amplifies the beneficial metabolic effects of antidiabetic rosiglitazone while blocking the weight-gaining effects of the drug.

Histological analysis reveals an increased frequency of multilocular adipocytes in iWAT depots of rosiglitazone-treated *Zfp423*-iAKO mice as compared with rosiglitazone-treated control animals (Fig. 7F–I). In fact, we observed very few iWAT multilocular adipocytes in obese control animals treated with rosiglitazone, whereas these beige-like adipocytes were readily detected in the treated *Zfp423*-iAKO mice (Fig. 7F–I). Quantitative gene expression analysis of the iWAT depots revealed a synergistic effect of rosiglitazone treatment and adipocyte *Zfp423* deficiency on the induction of the thermogenic gene program. In obese control mice (~40 g at the time of treatment), rosiglitazone stimulated the induction of *Ucp1* ~10-fold over baseline (vehicle) (Fig. 7J). Adipocyte *Zfp423* deletion alone results in induction in *Ucp1* mRNA levels also by ~10-fold (Fig. 7J). Notably, the induction of *Ucp1* expression in rosiglitazone-treated *Zfp423*-iAKO mice occurs by >100-fold (Fig. 7J). This robust effect of rosiglitazone on *Ucp1* expression in *Zfp423*-iAKO mice is in line with the biochemical observations that *Zfp423* deficiency leads to increased PPARγ occupancy at thermogenic genes and heightened transcriptional activity.

Discussion

Great progress has been made in identifying the transcriptional machinery that drives the thermogenic program of brown/beige adipocytes (Wang and Seale 2016). The data presented here highlight the key mechanisms that white adipocytes use to suppress this thermogenic gene program. *Zfp423* expression is enriched in white adipocytes as compared with thermogenic fat cells and is suppressed in adipocytes upon cold exposure or direct β-adrenergic stimulation (Shao et al. 2016). *Zfp423* expression then increases in beige cells upon cessation of cold stress as they return to a dormant/inactive state (Roh et al. 2018). As such, the modulation of *Zfp423* expression appears to represent a physiological switch that allows adipocytes to control their thermogenic plasticity. Collectively, our new data here point to a model in which ZFP423 acts to limit PPARγ occupancy at thermogenic genes in energy-storing white adipocytes by preventing EBF2-dependent chromatin remodeling. When *Zfp423* is lost from white adipocytes, EBF2 engages its transcriptional coactivators and facilitates chromatin remodeling and PPARγ occupancy in a manner akin to how it operates in the brown adipocyte lineage. In this study, we did not perform lineage tracing analysis of adipocytes in Adipo-*Zfp423*$^{H1285N\text{-}Avi}$

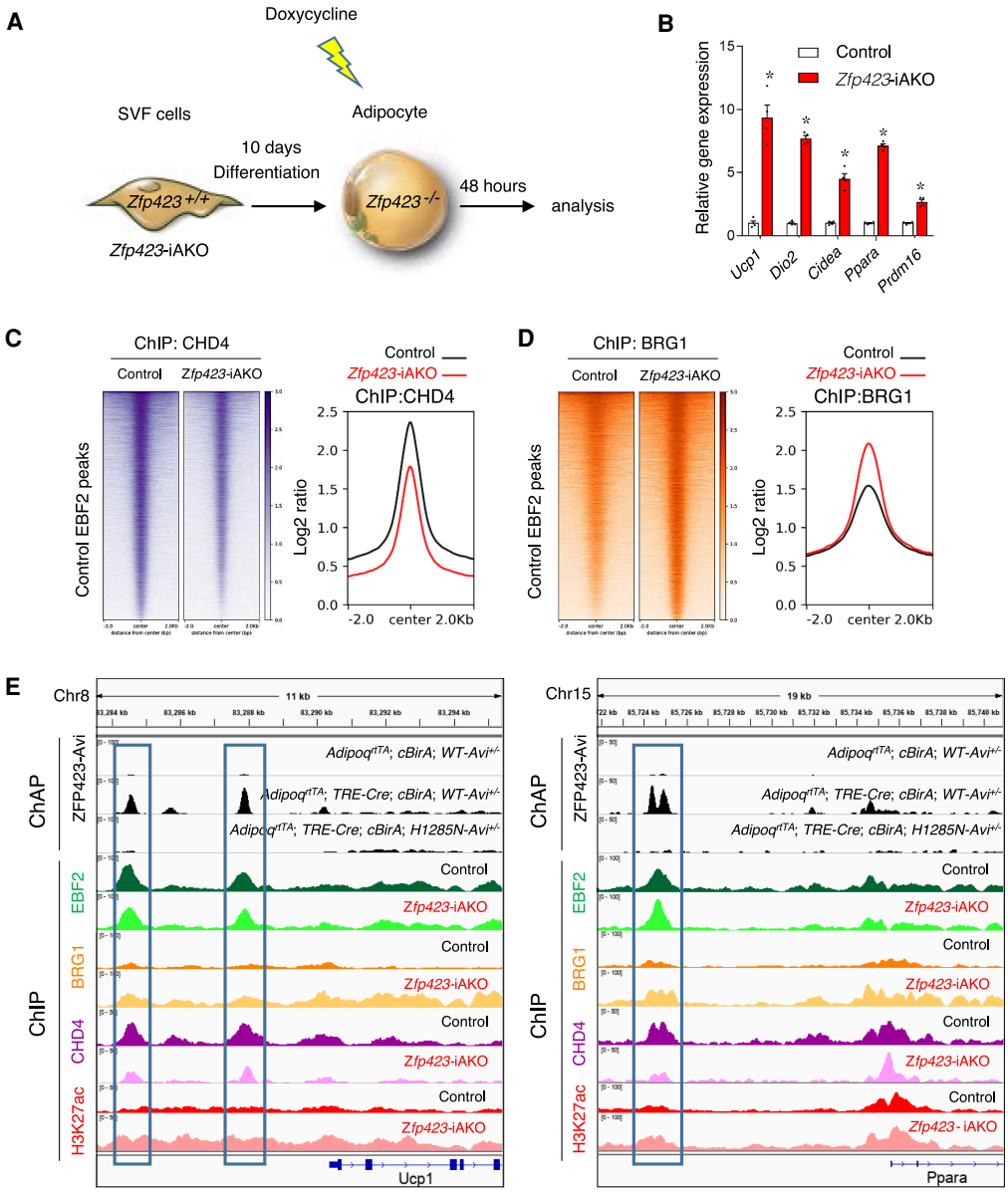

Figure 5. ZFP423 regulates EBF2 coregulator recruitment at EBF2 target genes. (*A*) Experimental design: iWAT SVF isolated from control or *Zfp423*-iAKO mice were induced to differentiate in vitro. Differentiated adipocytes were treated with 5 µM Dox for 12 h to inactivate *Zfp423*. Forty-eight hours after Dox treatment, cells were harvested for gene expression analysis or chromatin immunoprecipitation (ChIP) sequencing analyses. (*B*) Relative mRNA levels of the indicated thermogenic genes 48 h after Dox treatment of the differentiated adipocytes described in *A*. Bars represent mean + SEM. (*) $P < 0.05$ by Student's *t*-test. $n = 4$ biological replicates. (*C*) Heat map (*left*) and profile plot (*right*) illustrating CHD4 occupancy at EBF2-occupied regions in control and *Zfp423*-iAKO adipocytes. (*D*) Heat map (*left*) and profile plot (*right*) illustrating BRG1 occupancy at EBF2-occupied regions in control and *Zfp423*-iAKO adipocytes. (*E*) ZFP423 ChAP-seq signals and ChIP-seq signals for EBF2, BRG1, CHD4, and H3K27ac at the *Ucp1* and *Ppara* loci in control and *Zfp423*-iAKO adipocytes.

mice; however, our prior lineage tracing studies of *Zfp423*-iAKO mice indeed demonstrate that mature unilocular adiponectin-expressing adipocytes convert to multilocular UCP1-expressing cells when ZFP423 function is lost (Shao et al. 2016).

There is considerable interest in identifying strategies to promote brown adipose tissue activity to enhance weight loss and/or improve cardiometabolic health. Nevertheless, enthusiasm for targeting brown adipose tissue in obese individuals is tempered by numerous challenges. The amount of existing thermogenic adipose in adults appears quite variable, and obesity is associated with a significant reduction in the mass and activity of this tissue (Cypess et al. 2009; van Marken Lichtenbelt et al. 2009). Thus, fully activated classical brown adipose tissue in obese individuals may not exert a significant clinical

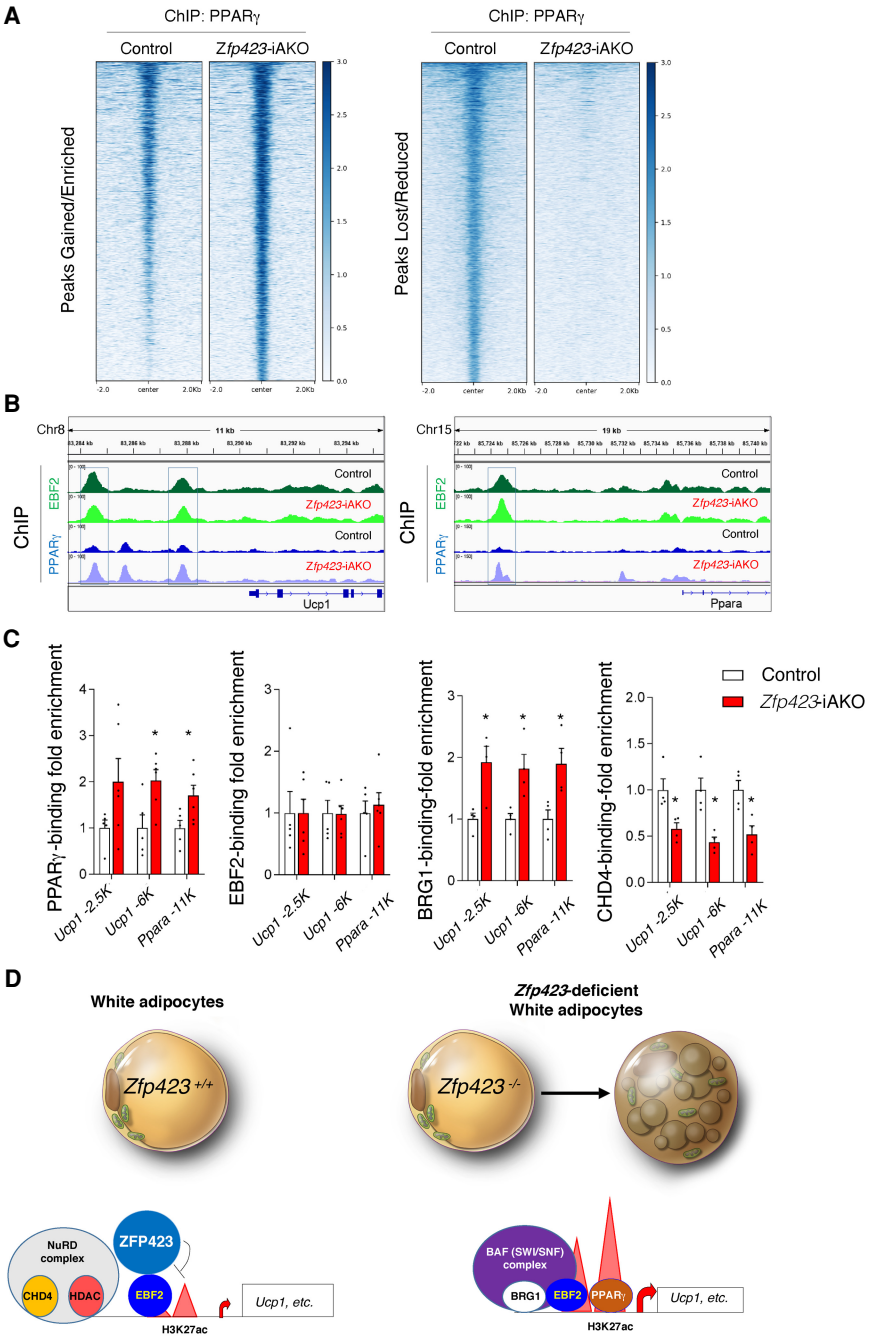

Figure 6. *Zfp423* deficiency leads to increased PPARγ occupancy at EBF2 target thermogenic genes. (*A*) Heat maps illustrating PPARγ occupancy in control and *Zfp423*-iAKO adipocytes. Genomic elements with quantitatively increased (*left*) or reduced (*right*) PPARγ occupancy in control and *Zfp423*-iAKO adipocytes are shown. (*B*) ChIP-seq signals for EBF2 and PPARγ at the *Ucp1* (*left*) and *Ppara* (*right*) loci in control and *Zfp423*-iAKO adipocytes. (*C*) ChIP-qPCR analysis of PPARγ, EBF2, BRG1, and CHD4 occupancy at the indicated EBF2-occupied regions at *Ucp1* and *Ppara* loci in control and *Zfp423*-iAKO adipocytes. Bars represent mean + SEM. (*) $P < 0.05$ by Student's *t*-test. $n = 5$ per genotype for PPARγ and EBF2 ChIP-qPCR analysis; $n = 4$ per genotype for BRG1 and CHD4 ChIP-qPCR analysis. (*D*) Proposed model: ZFP423 acts to limit PPARγ occupancy at thermogenic genes in energy-storing white adipocytes by preventing EBF2-dependent chromatin remodeling (H3K27 acetylation). When *Zfp423* is lost from white adipocytes, EBF2 engages its transcriptional coactivators and facilitates chromatin remodeling and PPARγ occupancy in a manner similar to how it operates in the brown adipocyte lineage. This facilitates the conversion of white adipocytes to a thermogenic phenotype.

effect, particularly in the face of counterregulatory mechanisms that help maintain body weight (e.g. increased food intake or WAT catecholamine resistance). Under physiological conditions, the β-adrenergic system represents the strongest activator of adipose thermogenesis. In rodents, agonists of the β3 adrenergic receptor robustly stimulate adipocyte thermogenesis. In human adipocytes, the β2 adrenergic receptor appears to be the key driver (Blondin et al. 2020). Use of the FDA-approved adrenergic receptor agonist, mirabegron (targeting both β2 and β3 adrenergic receptors at high doses), has shown promise as an activator of BAT in healthy humans (Cypess et al. 2015); however, the high doses of mirabegron required also come with a potential for unwanted side effects. The data presented here, along with our prior work, highlight the ability of mature white adipocytes to be converted into thermogenic adipocytes when transcriptional brakes are removed. It is tempting to speculate that efforts to release the "brakes" on thermogenic gene transcription while applying β-adrenergic receptor agonists or other "accelerators" of thermogenesis may thus represent a combinatorial strategy to enhance adipose thermogenic remodeling in obesity at lower doses of agonist. As case in point, we demonstrated that the loss of adipocyte

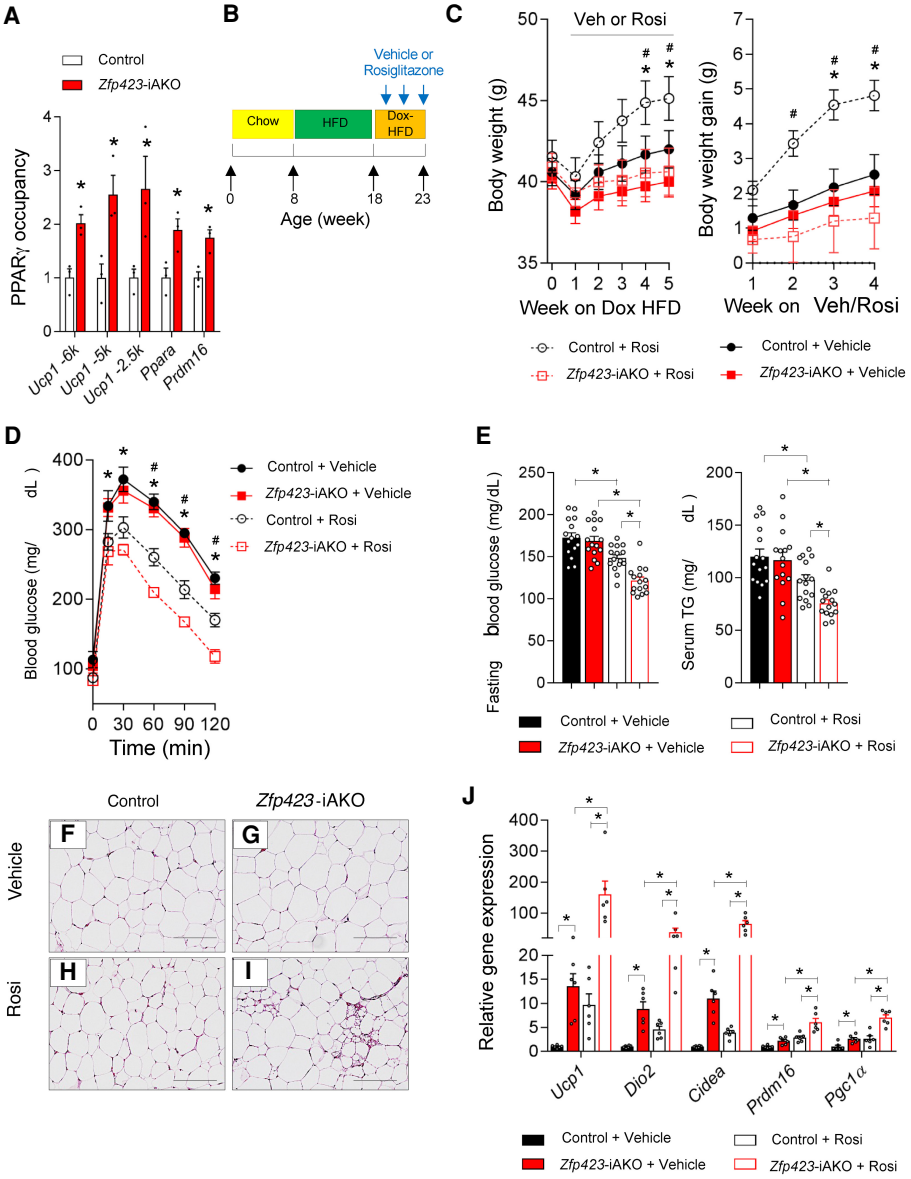

Figure 7. Adipocyte ZFP423 inactivation enhances the beneficial effects of thiazolidinediones in diet-induced obesity. (*A*) ChIP-qPCR analysis of PPARγ occupancy at the indicated EBF2-occupied regions of the *Ucp1*, *Ppara*, and *Prdm16* loci in whole iWAT isolated from control and *Zfp423*-iAKO mice after 4 wk of Dox-chow diet feeding. Bars represent mean + SEM. (*) $P < 0.05$ by Student's *t*-test. $n = 3$ biological replicates per genotype. (*B*) Experimental design: Eight-week-old control and *Zfp423*-iAKO mice were maintained on a 60% high-fat diet (HFD) for 10 wk before switching to Dox-HFD for another 5 wk. Vehicle or rosiglitazone (10 mg/kg/d) was delivered during the 5 wk of Dox-HFD feeding. (*C*) Average body weights and body weight gain of mice during Dox-HFD feeding. (*) $P < 0.05$ control + vehicle versus control + Rosi by two-way ANOVA, (#) $P < 0.05$ control + Rosi versus *Zfp423*-iAKO + Rosi by two-way ANOVA. $n = 15$ mice per group. (*D*) Glucose tolerance tests of control and *Zfp423*-iAKO mice after 4 wk of vehicle or rosiglitazone administration. (*) $P < 0.05$ control + vehicle versus control + Rosi by two-way ANOVA, (#) $P < 0.05$ for control + Rosi versus *Zfp423*-iAKO + Rosi by two-way ANOVA. $n = 7$ mice for vehicle groups; $n = 8$ mice for Rosi-treated groups. (*E*) Levels of fasting (6 h) blood glucose and serum triglycerides (TG) in control and *Zfp423*-iAKO mice after 4 wk of vehicle or rosiglitazone administration. Bars represent mean + SEM. (*) $P < 0.05$ by two-way ANOVA. $n = 15$ mice per group. (*F–I*) Representative bright-field images of H&E-stained iWAT sections from control and *Zfp423*-iAKO mice after 4 wk of vehicle or rosiglitazone administration. Scale bar, 200 µm. (*J*) Relative mRNA levels of the indicated thermogenic genes in iWAT from control and *Zfp423*-iAKO mice after 4 wk of vehicle or rosiglitazone administration. Bars represent mean + SEM. (*) $P < 0.05$ by two-way ANOVA. $n = 6$ per group.

ZFP423 results in a shift in PPARγ occupancy to thermogenic gene promoters in adipocytes and enables rosiglitazone to exert a stronger effect on the thermogenic gene program of WAT in vivo. Notably, this shift in PPARγ occupancy appears to amplify the beneficial metabolic effects of antidiabetic rosiglitazone while blocking the weight-gaining effects of the drug. Clinically, there is considerable variability in the response to thiazolidinedione

treatment (Sears et al. 2009). Remarkably, genetic variation that impacts PPARγ occupancy can predict the antidiabetic response to these drugs (Soccio et al. 2015; Hu et al. 2019). Although not directly tested here, it is possible that the antidiabetic effects of PPARγ agonists can be observed at lower doses with fewer side effects when their ability to drive WAT browning can be enhanced.

Targeting nonreceptor transcriptional components in a cell type-specific manner through conventional pharmacological strategies remains a tremendous challenge. *Zfp423* is also expressed in the adult brain, proliferating muscle satellite cells, and endothelial cells (Warming et al. 2006; Cheng et al. 2007; Cheng and Reed 2007; Gupta et al. 2012; Addison et al. 2019). As such, efforts to manipulate ZFP423 expression or activity itself could depend on the ability to selectively target adipocytes. Nevertheless, several recent studies have highlighted the promise of cell-based therapeutic approaches to increase thermogenic adipocyte mass in vivo. Patient-derived mesenchymal progenitors can be engineered to differentiate into a thermogenic adipocyte phenotype in vitro and then transplanted into animals to induce metabolic benefits (Min et al. 2016; Wang et al. 2020). Such approaches are still in their infancy; however, the promise of cell-based therapies highlights the possibility of using the knowledge of transcriptional mechanisms governing white and brown adipocyte differentiation to devise strategies to promote the expansion of thermogenic adipose tissue in humans.

Materials and methods

Animals

Adiponenctin^{rtTA}, *TRE-Cre*, and *Zfp423*$^{loxP/loxP}$ have been described previously (Shao et al. 2016). *Rosa26R*$^{lox\text{-}STOP\text{-}lox\text{-}BirA}$ mice were obtained from Jackson Laboratories (stock 030420) and were previously described (Johnson et al. 2017). *Zfp423*$^{WT\text{-}Avi}$ and *Zfp423*$^{H1285\text{-}Avi}$ mice were generated by the Children's Research Institute Mouse Genome Engineering Core at University of Texas Southwestern using CRISPR–Cas9 gene editing. Sequences of the gRNA and repair templates used are in the Supplemental Material. All animals used in this study were male and on a pure C57BL/6 background. Mice were maintained with a 12-h light/dark cycle and free access to food and water. All animal experiments were performed according to procedures approved by the University of Texas Southwestern Institutional Animal Care and Use Committee. Details regarding rodent diets are in the Supplemental Material.

Isolation of adipose stromal vascular fraction and in vitro adipogenesis

The stromal vascular fraction (SVF) of WAT was isolated by collagenase digestion as previously described (Shao et al. 2018). Freshly isolated inguinal WAT SVF cells were cultured in DMEM/F12 plus 10% FBS, pen/strep, and gentamicin (growth media). For in vitro differentiation, iWAT SVF cells were cultured in 10% CO_2 at 37°C until confluency. Confluent cultures were stimulated with adipogenic induction media (growth media supplemented with 5 µg mL^{-1} insulin, 1 µM dexamethasone, 0.5 mM isobutylmethyxanthine, 1 µM rosiglitazone) for 48 h. After induction, cells were maintained in growth media supplemented with 5 µg mL^{-1} insulin (maintenance media) for another 8 d until used for experiments.

Glucose tolerance tests and serum measurements

For glucose tolerance tests, mice were injected i.p. with glucose (1 g/kg body weight; Sigma) after an overnight fast. Blood was collected by venous bleeding from the tail vein at 0, 15, 30, 60, 90, and 120 min after injection. For measurements of fasting blood glucose, mice were fasted from 9:00 a.m. to 3:00 p.m. (6 h). All glucose concentrations were measured using Bayer Contour glucometers. Serum levels of triglycerides were determined using a triglyceride determination kit (triglyceride reagent T2449 and free glycerol reagent F6428; Sigma).

Retroviral production and transduction

Retrovirus was packaged in Phoenix cells as previously described (Gupta et al. 2010). Briefly, Phoenix packaging cells were cotransfected with 10 µg of the indicated pMSCV overexpression plasmids and 5 µg of gag-pol (Addgene 8449) and 5 µg of VSV (Addgene 8454) plasmids using Lipofectamine LTX (Thermo Fisher Scientific 15338100). Media containing viral particles were harvested 48 h after transfection and centrifuged at 600*g* for 5 min to clear debris. iWAT SVF cells isolated from control and *Zfp423*-iAKO mice were transduced with diluted virus-containing supernatants (1:1 ratio) in DMEM/F12 media containing 8 µg/mL polybrene (Sigma TR-1003) for 24 h. Following transduction, cells were maintained in fresh media for >48 h and then used for experiments.

Affinity purification and proteomics analysis

A stable cell line expressing *Zfp423* was generated by drug selection of immortalized brown SVF cells transduced with pMSCV-Puro-^{FLAG}-ZFP423 plasmids. *Zfp423*-overexpressing cells were lysed in Pierce IP lysis buffer (Thermo Fisher Scientific 87787) supplemented with protease inhibitor cocktail (Sigma P8340). Cell lysate was incubated with anti-FLAG (Sigma, F1804) or normal IgG (Cell Signaling Technology 2729) overnight at 4°C. Lysates were then incubated with Protein G Sepharose 4 Fast Flow (GE Healthcare Biosciences 17-0618-01) for 2 h at 4°C to capture immune complexes. Purified immune complexes were washed sequentially three times with washing buffer (50 mM HEPES at pH 7.4, 10% glycerol, 0.05% NP40, 1 mM DTT, 0.25 mM PMSF, 150 mM KCl) supplemented with protease inhibitor cocktail (Sigma P8340). Proteins were eluted with Pierce IgG elution buffer (Thermo Fisher Scientific 21004) and briefly resolved by SDS-PAGE prior to the submission to the University of Texas Southwestern Proteomics Core. Details regarding proteomics analysis are in the Supplemental Material.

Coimmunoprecipitation assay

Coimmunoprecipitation was performed as previously described (Shao et al. 2016). In brief, cells were lysed in Pierce IP lysis buffer (Thermo Fisher Scientific 87787) supplemented with 1% protease inhibitor cocktail (Sigma 8340). Following the overnight incubation with the indicated antibodies at 4°C, the cell lysates were mixed with Protein G Sepharose 4 Fast Flow (GE Healthcare Biosciences 17-0618-01) for 1 h at room temperature to capture immune complexes. After three sequential washes with Pierce IP lysis buffer, samples were eluted by boiling in 2× SDS loading buffer and resolved by SDS-polyacrylamide gel electrophoresis (SDS-PAGE) and immunoblotting.

Gene expression analysis

Total RNA from tissue or cells was extracted and purified using the TRIzol reagent (Invitrogen) and the RNeasy mini kit (Qiagen). Total RNA from FACS-sorted cells was extracted using RNAqueous microRNA isolation kit (Thermo Fisher Scientific). cDNA was synthesized with M-MLV reverse transcriptase (Invitrogen) and random hexamer primers (Invitrogen). Relative expression of mRNAs was determined by quantitative PCR using SYBR Green PCR system (Applied Biosystems), and values were normalized to levels of *Rps18* using the ΔΔ-Ct method. All qPCR primer sequences are listed in Supplemental Table S5.

Histological analysis

Dissected tissues were fixed in 4% paraformaldehyde overnight. Paraffin embedding, sectioning, and H&E staining were performed at the Molecular Pathology Core Facility at University of Texas Southwestern. Bright-field images were acquired using a Keyence BZ-X710 microscope.

Immunoblotting

Protein extracts from cells or tissues were prepared by homogenization in RIPA lysis buffer (Santa Cruz Biotechnology) supplemented with protease inhibitor cocktail (Sigma P8340), and phosphatase inhibitor cocktails (Sigma P5726 and P0044). Protein extracts were separated by SDS-PAGE electrophoresis and transferred onto PVDF membrane (Millipore IPFL00010). After incubation with the indicated primary antibodies overnight at 4°C, the blots were incubated with IR dye- coupled secondary antibodies (LI-COR) and visualized by the LI-COR Odyssey infrared imaging system. Details regarding antibodies and working concentrations are in the Supplemental Material.

Cross-linking

Cross-linking for ChIP or ChAP was performed as described (Shan et al. 2020). iWAT SVF isolated from the indicated animals were induced to differentiate in vitro. Differentiated adipocytes were treated with 5 μM Dox for 12 h to induce rtTA/CRE activity. Forty-eight hours after Dox treatment, cells were cross-linked with 1% formaldehyde in PBS for 10 min at 37°C and quenched in 125 mM glycine in PBS for 5 min at 4°C. For tissue ChIP, iWAT depots isolated from control or *Zfp423*-iAKO mice after 4 wk of Dox-chow diet feeding were diced into small pieces (~5 mm^3), fixed with 1% formaldehyde in PBS for 10 min at 37°C, and quenched in 125 mM glycine in PBS for 5 min at 4°C. Details regarding ChIP assays and library production are in the Supplemental Material.

Chromatin ffinity purifications (ChAPs)

Cross-linked cells and tissues were lysed in Farnham lysis buffer (5 mM PIPES at pH 8.0, 85 mM KCl, 0.5% NP-40, 1 mM DTT, protease inhibitor cocktail [Sigma P8340]) to obtain nuclear material. Crude nuclear pellets were collected by centrifugation and then lysed by incubation in lysis buffer containing 5 mM Tris-HCl (pH 7.9), 1% SDS, 10 mM EDTA, 1 mM DTT, and protease inhibitor cocktail (Sigma P8340). Chromatin fragmentation (200- to 500-bp length) was performed at 4°C by a Bioruptor 300 using the setting of 10 cycles of 30 sec on and 60 sec off. Soluble chromatin was diluted 1:10 with dilution buffer (20 mM Tris-HCl at pH 7.9, 1% Triton X-100, 2 mM EDTA, 150 mM NaCl, 0.1% SDS, protease inhibitor cocktail [Sigma P8340]) and precleared using Streptavidin Sepharose high-performance beads (GE Healthcare Biosciences 17-5113-01) for 1 h at 4°C. Precleared samples were incubated with the streptavidin sepharose beads for 2 h at 4°C. Affinity-purified material was consecutively washed with SDS wash buffer (2% SDS in 50 mM Tris-HCl at pH 7.9, protease inhibitor cocktail [Sigma P8340]) twice, high-salt wash buffer (50 mM Tris-HCl at pH 7.9, 1 mM EDTA, 500 mM NaCl, 0.1% sodium deoxycholate, 1% Triton X-100, protease inhibitor cocktail [Sigma P8340]), LiCl wash buffer (10 mM Tris-HCl at pH 7.9, 1 mM EDTA, 250 mM LiCl, 0.5% NP-40, 0.5% sodium deoxycholate, protease inhibitor cocktail [Sigma P8340]), and 1× Tris-EDTA (TE). After elution at SDS elution buffer (50 mM Tris-Hcl at pH 7.9, 1% SDS, 10 mM EDTA) overnight at 70°C, the affinity-purified material was digested with RNase (Roche 11119915001) and proteinase K (Thermo Fisher Scientific EO0491) prior to the purification and concentration of the affinity-purified genomic DNA by ChIP DNA Clean & Concentrator kit (Zymo Research D5201). ChAP-isolated DNA was subjected to library production (ChAP-seq) using NEBnext NGS DNA library preparation for Illumina kit (New England Biolabs E7645). Sequencing was performed with Illumina NextSeq 500 mid output (130M) by the University of Texas Southwestern McDermott Center Next-Generation Sequencing Core. ChIP/ChAP-seq analysis was performed as previously described (Shan et al. 2020). Details regarding these analyses are in the Supplemental Material.

Quantification and statistical analysis

All data were expressed as the mean + SEM. We used GraphPad Prism 7.0 (GraphPad Software, Inc.) to perform the statistical analyses. For comparisons between two independent groups, a Student's *t*-test was used and $P < 0.05$ was considered statistically significant. For in vitro studies, we estimated the approximate effect size based on independent preliminary studies. Studies designed to characterize an in vitro difference in gene expression were estimated to have a slightly larger effect size of 30% with assumed 15% standard deviation of group means. To detect this difference at a power of 80% and an α of 0.05, we predicted we would need four independent replicates per group. We estimated this effect size based on independent preliminary studies. Statistical information, including *P*-values, samples sizes, and repetitions, for all data sets are in Supplemental Data Set S6.

Material and data availability

The ChIP and ChAP sequencing data sets are available at GEO accession viewer (https://www.ncbi.nlm.nih.gov/geo) under the accession numbers GSE175653 and GSE175654. The mass spectrometry data sets are available at MassIVE (https://massive.ucsd.edu) under the accession number MSV000087563.

Competing interest statement

The authors declare no competing interests.

Acknowledgments

We are grateful to members of the University of Texas Southwestern Touchstone Diabetes Center for useful discussions. We thank Charlotte Lee, the University of Texas Southwestern Animal Resource Center, Metabolic Phenotyping Core, Pathology Core, Live-Cell Imaging Core, Flow Cytometry Core, and McDermott Sequencing Center for excellent guidance and assistance with experiments performed here. We thank the University of Texas

Southwestern Children's Research Institute Mouse Genome Engineering Core for generating the *Zfp423*$^{WT\text{-}Avi}$ and *Zfp423*$^{H1285\text{-}Avi}$ genetic strains. This study and/or personnel were supported in part by National Institutes of Health National Institute of Diabetes and Digestive and Kidney Diseases (NIDDK) R01 DK104789, R01 DK119163, and RC2 DK118620 to R.K.G.; American Heart Association postdoctoral fellowship 16POST26420136 and Career Development Award 19CDA34670007 from the American Heart Association and the Harry S. Moss Heart Trust to M.S.; and NIDDK R01 DK121801 and DK123356 to P.S.

Author contributions: M.S. and R.K.G. conceived the study and wrote the manuscript. M.S. and R.K.G. designed experiments. L.L. and M.S. designed genetic targeting strategies. M.S., Q.Z., A.T. B.S., and L.V. performed experiments. P.S. contributed essential reagents and edited the manuscript. All authors analyzed the data.

References

Addison WN, Hall KC, Kokabu S, Matsubara T, Fu MM, Gori F, Baron R. 2019. Zfp423 regulates skeletal muscle regeneration and proliferation. *Mol Cell Biol* **39:** e00447-18. doi:10.1128/MCB.00447-18

Alcaraz WA, Gold DA, Raponi E, Gent PM, Concepcion D, Hamilton BA. 2006. Zfp423 controls proliferation and differentiation of neural precursors in cerebellar vermis formation. *Proc Natl Acad Sci* **103:** 19424–19429. doi:10.1073/pnas.0609184103

Barbatelli G, Murano I, Madsen L, Hao Q, Jimenez M, Kristiansen K, Giacobino JP, De Matteis R, Cinti S. 2010. The emergence of cold-induced brown adipocytes in mouse white fat depots is determined predominantly by white to brown adipocyte transdifferentiation. *Am J Physiol Endocrinol Metab* **298:** E1244–E1253. doi:10.1152/ajpendo.00600.2009

Becher T, Palanisamy S, Kramer DJ, Eljalby M, Marx SJ, Wibmer AG, Butler SD, Jiang CS, Vaughan R, Schöder H, et al. 2021. Brown adipose tissue is associated with cardiometabolic health. *Nat Med* **27:** 58–65. doi:10.1038/s41591-020-1126-7

Beckett D, Kovaleva E, Schatz PJ. 1999. A minimal peptide substrate in biotin holoenzyme synthetase-catalyzed biotinylation. *Protein Sci* **8:** 921–929. doi:10.1110/ps.8.4.921

Blondin DP, Nielsen S, Kuipers EN, Severinsen MC, Jensen VH, Miard S, Jespersen NZ, Kooijman S, Boon MR, Fortin M, et al. 2020. Human brown adipocyte thermogenesis is driven by β2-AR stimulation. *Cell Metab* **32:** 287–300.e7. doi:10.1016/j.cmet.2020.07.005

Cheng LE, Reed RR. 2007. Zfp423/OAZ participates in a developmental switch during olfactory neurogenesis. *Neuron* **54:** 547–557. doi:10.1016/j.neuron.2007.04.029

Cheng LE, Zhang J, Reed RR. 2007. The transcription factor Zfp423/OAZ is required for cerebellar development and CNS midline patterning. *Dev Biol* **307:** 43–52. doi:10.1016/j.ydbio.2007.04.005

Cypess AM, Lehman S, Williams G, Tal I, Rodman D, Goldfine AB, Kuo FC, Palmer EL, Tseng YH, Doria A, et al. 2009. Identification and importance of brown adipose tissue in adult humans. *N Engl J Med* **360:** 1509–1517. doi:10.1056/NEJMoa0810780

Cypess AM, Weiner LS, Roberts-Toler C, Franquet Elía E, Kessler SH, Kahn PA, English J, Chatman K, Trauger SA, Doria A, et al. 2015. Activation of human brown adipose tissue by a β3-adrenergic receptor agonist. *Cell Metab* **21:** 33–38. doi:10.1016/j.cmet.2014.12.009

Gupta RK, Arany Z, Seale P, Mepani RJ, Ye L, Conroe HM, Roby YA, Kulaga H, Reed RR, Spiegelman BM. 2010. Transcriptional control of preadipocyte determination by Zfp423. *Nature* **464:** 619–623. doi:10.1038/nature08816

Gupta RK, Mepani RJ, Kleiner S, Lo JC, Khandekar MJ, Cohen P, Frontini A, Bhowmick DC, Ye L, Cinti S, et al. 2012. Zfp423 expression identifies committed preadipocytes and localizes to adipose endothelial and perivascular cells. *Cell Metab* **15:** 230–239. doi:10.1016/j.cmet.2012.01.010

Harms M, Seale P. 2013. Brown and beige fat: development, function and therapeutic potential. *Nat Med* **19:** 1252–1263. doi:10.1038/nm.3361

Hata A, Seoane J, Lagna G, Montalvo E, Hemmati-Brivanlou A, Massagué J. 2000. OAZ uses distinct DNA- and protein-binding zinc fingers in separate BMP-Smad and Olf signaling pathways. *Cell* **100:** 229–240. doi:10.1016/S0092-8674(00)81561-5

Hepler C, Shao M, Xia JY, Ghaben AL, Pearson MJ, Vishvanath L, Sharma AX, Morley TS, Holland WL, Gupta RK. 2017. Directing visceral white adipocyte precursors to a thermogenic adipocyte fate improves insulin sensitivity in obese mice. *Elife* **6:** e27669. doi:10.7554/eLife.27669

Hu W, Jiang C, Guan D, Dierickx P, Zhang R, Moscati A, Nadkarni GN, Steger DJ, Loos RJF, Hu C, et al. 2019. Patient adipose stem cell-derived adipocytes reveal genetic variation that predicts antidiabetic drug response. *Cell Stem Cell* **24:** 299–308.e6. doi:10.1016/j.stem.2018.11.018

Johnson BS, Zhao YT, Fasolino M, Lamonica JM, Kim YJ, Georgakilas G, Wood KH, Bu D, Cui Y, Goffin D, et al. 2017. Biotin tagging of MeCP2 in mice reveals contextual insights into the Rett syndrome transcriptome. *Nat Med* **23:** 1203–1214. doi:10.1038/nm.4406

Kajimura S, Spiegelman BM, Seale P. 2015. Brown and beige fat: physiological roles beyond heat generation. *Cell Metab* **22:** 546–559. doi:10.1016/j.cmet.2015.09.007

Lauberth SM, Rauchman M. 2006. A conserved 12-amino acid motif in Sall1 recruits the nucleosome remodeling and deacetylase corepressor complex. *J Biol Chem* **281:** 23922–23931. doi:10.1074/jbc.M513461200

Lee YH, Petkova AP, Konkar AA, Granneman JG. 2015. Cellular origins of cold-induced brown adipocytes in adult mice. *FASEB J* **29:** 286–299. doi:10.1096/fj.14-263038

Lončar D. 1991. Convertible adipose tissue in mice. *Cell Tissue Res* **266:** 149–161. doi:10.1007/BF00678721

Min SY, Kady J, Nam M, Rojas-Rodriguez R, Berkenwald A, Kim JH, Noh HL, Kim JK, Cooper MP, Fitzgibbons T, et al. 2016. Human 'brite/beige' adipocytes develop from capillary networks, and their implantation improves metabolic homeostasis in mice. *Nat Med* **22:** 312–318. doi:10.1038/nm.4031

Mota de Sa P, Richard AJ, Hang H, Stephens JM. 2017. Transcriptional regulation of adipogenesis. *Compr Physiol* **7:** 635–674.

Pearson S, Loft A, Rajbhandari P, Simcox J, Lee S, Tontonoz P, Mandrup S, Villanueva CJ. 2019. Loss of TLE3 promotes the mitochondrial program in beige adipocytes and improves glucose metabolism. *Genes Dev* **33:** 747–762. doi:10.1101/gad.321059.118

Rajakumari S, Wu J, Ishibashi J, Lim HW, Giang AH, Won KJ, Reed RR, Seale P. 2013. EBF2 determines and maintains brown adipocyte identity. *Cell Metab* **17:** 562–574. doi:10.1016/j.cmet.2013.01.015

Roby YA, Bushey MA, Cheng LE, Kulaga HM, Lee SJ, Reed RR. 2012. Zfp423/OAZ mutation reveals the importance of Olf/EBF transcription activity in olfactory neuronal maturation. *J Neurosci* **32:** 13679–13688a. doi:10.1523/JNEUROSCI.6190-11.2012

Roh HC, Tsai LTY, Shao M, Tenen D, Shen Y, Kumari M, Lyubetskaya A, Jacobs C, Dawes B, Gupta RK, et al. 2018. Warming induces significant reprogramming of beige, but not brown, adipocyte cellular identity. *Cell Metab* **27:** 1121–1137.e5. doi:10.1016/j.cmet.2018.03.005

Rosen ED, Spiegelman BM. 2014. What we talk about when we talk about fat. *Cell* **156:** 20–44. doi:10.1016/j.cell.2013.12.012

Rosenwald M, Perdikari A, Rülicke T, Wolfrum C. 2013. Bi-directional interconversion of brite and white adipocytes. *Nat Cell Biol* **15:** 659–667. doi:10.1038/ncb2740

Seale P, Conroe HM, Estall J, Kajimura S, Frontini A, Ishibashi J, Cohen P, Cinti S, Spiegelman BM. 2011. Prdm16 determines the thermogenic program of subcutaneous white adipose tissue in mice. *J Clin Invest* **121:** 96–105. doi:10.1172/JCI44271

Sears DD, Hsiao G, Hsiao A, Yu JG, Courtney CH, Ofrecio JM, Chapman J, Subramaniam S. 2009. Mechanisms of human insulin resistance and thiazolidinedione-mediated insulin sensitization. *Proc Natl Acad Sci* **106:** 18745–18750. doi:10.1073/pnas.0903032106

Shan B, Shao M, Zhang Q, Hepler C, Paschoal VA, Barnes SD, Vishvanath L, An YA, Jia L, Malladi VS, et al. 2020. Perivascular mesenchymal cells control adipose-tissue macrophage accrual in obesity. *Nat Metab* **2:** 1332–1349. doi:10.1038/s42255-020-00301-7

Shao M, Gupta RK. 2019. Transcriptional brakes on the road to adipocyte thermogenesis. *Biochim Biophys Acta Mol Cell Biol Lipids* **1864:** 20–28. doi:10.1016/j.bbalip.2018.05.010

Shao M, Ishibashi J, Kusminski CM, Wang QA, Hepler C, Vishvanath L, MacPherson KA, Spurgin SB, Sun K, Holland WL, et al. 2016. Zfp423 maintains white adipocyte identity through suppression of the beige cell thermogenic gene program. *Cell Metab* **23***:* 1167–1184. doi:10.1016/j.cmet.2016.04.023

Shao M, Vishvanath L, Busbuso NC, Hepler C, Shan B, Sharma AX, Chen S, Yu X, An YA, Zhu Y, et al. 2018. De novo adipocyte differentiation from Pdgfrβ$^+$ preadipocytes protects against pathologic visceral adipose expansion in obesity. *Nat Commun* **9:** 890. doi:10.1038/s41467-018-03196-x

Shao M, Wang QA, Song A, Vishvanath L, Busbuso NC, Scherer PE, Gupta RK. 2019. Cellular origins of beige Fat cells revisited. *Diabetes* **68:** 1874–1885. doi:10.2337/db19-0308

Shapira SN, Seale P. 2019. Transcriptional control of brown and beige fat development and function. *Obesity* **27:** 13–21. doi:10.1002/oby.22334

Shapira SN, Lim HW, Rajakumari S, Sakers AP, Ishibashi J, Harms MJ, Won KJ, Seale P. 2017. EBF2 transcriptionally regulates brown adipogenesis via the histone reader DPF3 and the BAF chromatin remodeling complex. *Genes Dev* **31:** 660–673. doi:10.1101/gad.294405.116

Soccio RE, Chen ER, Rajapurkar SR, Safabakhsh P, Marinis JM, Dispirito JR, Emmett MJ, Briggs ER, Fang B, Everett LJ, et al. 2015. Genetic variation determines PPARγ function and anti-diabetic drug response in vivo. *Cell* **162:** 33–44. doi:10.1016/j.cell.2015.06.025

Stine RR, Shapira SN, Lim HW, Ishibashi J, Harms M, Won KJ, Seale P. 2016. EBF2 promotes the recruitment of beige adipocytes in white adipose tissue. *Mol Metab* **5:** 57–65. doi:10.1016/j.molmet.2015.11.001

Torchy MP, Hamiche A, Klaholz BP. 2015. Structure and function insights into the NuRD chromatin remodeling complex. *Cell Mol Life Sci* **72:** 2491–2507. doi:10.1007/s00018-015-1880-8

van Marken Lichtenbelt WD, Vanhommerig JW, Smulders NM, Drossaerts JM, Kemerink GJ, Bouvy ND, Schrauwen P, Teule GJ. 2009. Cold-activated brown adipose tissue in healthy men. *New England Journal of Medicine* **360:** 1500–1508. doi:10.1056/NEJMoa0808718

Villanueva CJ, Vergnes L, Wang J, Drew BG, Hong C, Tu Y, Hu Y, Peng X, Xu F, Saez E, et al. 2013. Adipose subtype-selective recruitment of TLE3 or Prdm16 by PPARγ specifies lipid storage versus thermogenic gene programs. *Cell Metab* **17:** 423–435. doi:10.1016/j.cmet.2013.01.016

Vishvanath L, MacPherson KA, Hepler C, Wang QA, Shao M, Spurgin SB, Wang MY, Kusminski CM, Morley TS, Gupta RK. 2016. Pdgfrβ$^+$ mural preadipocytes contribute to adipocyte hyperplasia induced by high-fat-diet feeding and prolonged cold exposure in adult mice. *Cell Metab* **23:** 350–359. doi:10.1016/j.cmet.2015.10.018

Wang W, Seale P. 2016. Control of brown and beige fat development. *Nat Rev Mol Cell Biol* **17:** 691–702. doi:10.1038/nrm.2016.96

Wang ZV, Deng Y, Wang QA, Sun K, Scherer PE. 2010. Identification and characterization of a promoter cassette conferring adipocyte-specific gene expression. *Endocrinology* **151:** 2933–2939. doi:10.1210/en.2010-0136

Wang QA, Tao C, Gupta RK, Scherer PE. 2013. Tracking adipogenesis during white adipose tissue development, expansion and regeneration. *Nat Med* **19:** 1338–1344. doi:10.1038/nm.3324

Wang W, Kissig M, Rajakumari S, Huang L, Lim HW, Won KJ, Seale P. 2014. Ebf2 is a selective marker of brown and beige adipogenic precursor cells. *Proc Natl Acad Sci* **111:** 14466–14471. doi:10.1073/pnas.1412685111

Wang CH, Lundh M, Fu A, Kriszt R, Huang TL, Lynes MD, Leiria LO, Shamsi F, Darcy J, Greenwood BP, et al. 2020. CRISPR-engineered human brown-like adipocytes prevent diet-induced obesity and ameliorate metabolic syndrome in mice. *Sci Transl Med* **12:** eaaz8664. doi:10.1126/scitranslmed.aaz8664

Warming S, Rachel RA, Jenkins NA, Copeland NG. 2006. *Zfp423* is required for normal cerebellar development. *Mol Cell Biol* **26:** 6913–6922. doi:10.1128/MCB.02255-05

Wu J, Boström P, Sparks LM, Ye L, Choi JH, Giang AH, Khandekar M, Virtanen KA, Nuutila P, Schaart G, et al. 2012. Beige adipocytes are a distinct type of thermogenic fat cell in mouse and human. *Cell* **150:** 366–376. doi:10.1016/j.cell.2012.05.016